# Spectroscopic, Electrochemical, and Kinetic Trends in Fe(III)–Thiolate Autoredox Reactions Near Physiological pH

*Levi A. Ekanger,* Ruhi K. Shah, Matthew E. Porowski, Zach Ziolkowski, and Alana Calello*

Department of Chemistry, The College of New Jersey, Ewing, NJ 08628, United States

**ABSTRACT**

Substrate binding modes at thiol dioxygenase active sites have received increasing attention to better understand how selectivity and activation is achieved. Of particular interest is the substrate-binding mode within cysteamine dioxygenase (ADO) because of its unique selectivity for both cysteamine and N-terminal cysteine residues. ADO also exhibits unique reactivity with both substrates through an autoredox reaction of the form ADO-Fe(III)-SR → ADO-Fe(II) + ½ RSSR which is proposed to maintain Fe(II) under oxidative stress conditions. Here we use the complex [Fe(tacn)$Cl_3$] (tacn = 1,4,7-triazacyclononane) to replicate the 3N facial coordination environment in ADO-Fe(III) and to enable experiments buffered near physiological pH. Autoredox reactions are initiated by forming Fe(III)–thiolate intermediates *in situ* using cysteamine and cysteamine analogues penicillamine, mercaptopropionate, cysteine, *N*-acetylcysteine, and *N*-acetylcysteine methyl ester. We observe trends in UV–vis absorption

maxima, autoredox rate constants, and cathodic peak potentials as a function of substrate binding mode. Moreover, we observe autoredox reactivity on the same timescale reported for ADO autoredox activity. To provide evidence of tridentate coordination in the relatively reactive cysteine intermediate, we isolated a stable penicillamine-containing intermediate and characterized its coordination environment and electronic structure using FT-IR, NMR, and magnetic susceptibility measurements.

## INTRODUCTION

Thiol dioxygenases are central to life processes including cysteine homeostasis and taurine biosynthesis. Enzymatic activity of thiol dioxygenases, such as cysteine dioxygenase (CDO) and cysteamine dioxygenase (ADO), transform biological thiols into sulfinates through the activation of molecular oxygen.[1–8] Thiol dioxygenase active sites feature mononuclear non-heme Fe bound by three histidine residues forming a facial 3N binding mode (Figure 1A). The remaining three coordination sites on Fe are either occupied by three water molecules in the absence of substrate or by a combination of thiol substrate, water, or dioxygen. Within the CDO active site cysteine only binds to Fe through thiolate S and amine N atoms (S-N, Figure 1B).[9,10] Selectivity for S-N binding in CDO is noteworthy because coordination of cysteine to Fe can theoretically be accomplished in alternate binding modes. An alternate bidentate mode uses thiolate S and carboxylate O atoms (S-O), and a tridentate interaction arises from cysteine S, N, and O atoms from all three functional groups (S-N-O). The S-N binding mode in CDO is enforced by a highly conserved arginine residue that prevents cysteinyl carboxylate from coordinating to Fe. It therefore appears CDO evolved to selectively bind cysteine in the S-N binding mode by preventing S-O and S-N-O binding modes. While substrate binding mode is well understood at the CDO active site, it

is less understood for other thiol dioxygenases including mercaptopropionate dioxygenase (MDO) and ADO.

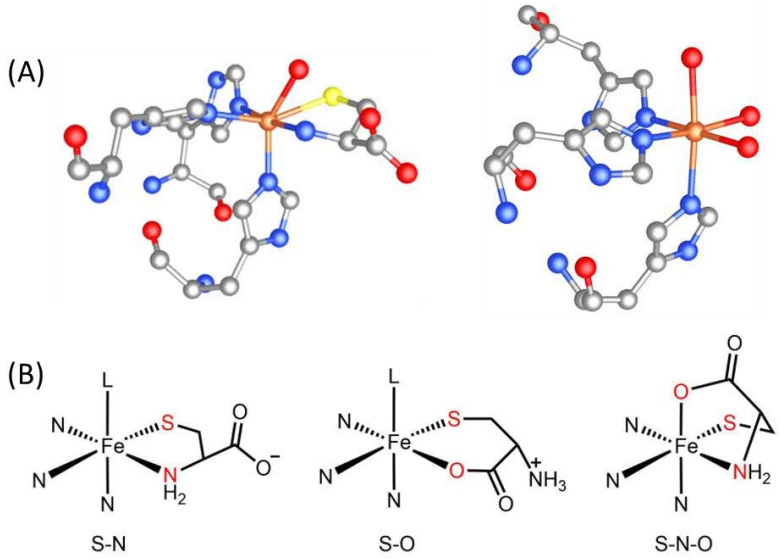


**Figure 1.** (A) Simplified coordination environments at CDO (left) and ADO (right) active sites. Cysteine is bound to CDO in the S-N mode while ADO contains no substrate. Protein crystal structures PDB: 4Z82 and PDB: 7LVZ were used for CDO and ADO, respectively. (B) Representation of S-N, S-O, and S-N-O binding modes in a 3N facial coordination environment with metal-bound heteroatoms colored in red.

Counterexamples to the S-N binding mode in CDO might be found at the MDO and ADO active sites. The presence of only thiol and carboxylate groups in mercaptopropionate leave S-O binding as the only multidentate interaction with Fe in MDO. However, both S-O binding and monodentate thiolate binding have been proposed for the MDO active site.[1,11,12] For these reasons there is growing interest in determining how thiol dioxygenases bind substrates to achieve selective thiol oxygenation as exemplified by recent studies focused on ADO.[4,5,7,13]

The activity of ADO is unique among thiol dioxygenases because both cysteamine and peptides with N-terminal cysteine residues are oxygenated to sulfinates by the metalloenzyme.[14] Common structural features of cysteamine and N-terminal cysteine residues are thiol and amine groups making the S-N binding mode a plausible hypothesis. An ADO model complex featuring a tris(pyrazolyl)borate supporting ligand binds cysteamine in the S-N mode and catalyzes S dioxygenation.[15] However, recent spectroscopic evidence suggests monodentate thiolate binding at the ADO active site like the purported interaction in MDO.[4] As of the writing of this manuscript structural data for substrate denticity at MDO and ADO active sites are unreported. In addition to catalyzing thiolate-to-sulfinate transformations, ADO exhibits autoredox chemistry.

Autoredox reactivity might have a role in ADO function. Recently characterized autoredox activity of ADO could induce enzyme reactivation through the reduction of Fe(III) to Fe(II) with concomitant thiolate-to-disulfide transformation. This reactivity has been documented between ADO and its natural substrates cysteamine and the N-terminus of regulator of G signaling 5 (RGS5), which likely undergo autoredox following the general reaction ADO-Fe(III)-SR → ADO-Fe(II) + ½ RSSR.[13] Autoredox might maintain ADO in its reduced state to preserve catalytic activity even under oxidative stress conditions. Interestingly, the autoredox product cysteamine disulfide, also known as cystamine, is an important biomolecule that disrupts bacterial metabolism and sensitizes *P. aeruginosa* to oxidative and nitrosative stress.[16] Given the importance of substrate binding mode at thiol dioxygenase active sites and the autoredox activity of ADO, we sought to investigate the effect of substrate binding modes on Fe(III)–thiolate autoredox rates and reduction potentials. To investigate how binding modes affect autoredox rates, we elected to pursue model chemistry using an Fe complex that replicates some structural features of thiol dioxygenase active sites.

Early model chemistry studies focused on Fe(III)-cysteine and related Fe(III)–thiolate interactions that form colorful intermediates from S→Fe(III) charge transfer transitions. It is well documented that Fe(III)–thiolate intermediates decay to colorless products under aerobic or anaerobic conditions consistent with an autoredox process. Transient formation of colorful intermediates enables colorimetric kinetic analyses to quantify their rates of formation and disappearance. For example, the kinetics of Fe(III)-cysteine and -thiolate interactions have been studied using simple (i.e. non-chelated) Fe(III) salts in acidic or alkaline media.[17–20] A consistent observation among prior studies is the formation of disulfides following second-order kinetics. Moreover, both early and modern studies use cysteine analogues, such as cysteamine and mercaptopropionate, to study the effect of substrate binding mode on electronic structure and reactivity.[20,21]

Prior studies on the anaerobic oxidation of cysteine by Fe(III) have experimental limitations that do not fit within the context of ADO autoredox chemistry. First, the use of non-chelated Fe(III) ions in prior studies do not replicate the 3N facial coordination environment of thiol dioxygenases. Second, the use of non-chelated Fe(III) ions necessitates the use of acidic or alkaline reaction solutions to prevent Fe(III)–hydroxide olation and precipitation near neutral pH values. The use of either highly acidic or alkaline pH values are not ideal considering substrate binding occurs in a physiologically relevant pH range in thiol dioxygenases. For example, CDO binds cysteine optimally at pH ~7.4.[3] Accordingly, the use of chelated Fe(III) is required to mimic the thiol dioxygenase active site and to enable studies in solutions buffered in a physiologically relevant pH range.

Motivated by early studies of Fe(III)-cysteine reaction kinetics, we turned to contemporary studies focused on CDO model chemistry to identify a suitable ligand for our studies. The CDO

active site is commonly modeled using tridentate ligands with nitrogen donor atoms to replicate the 3N facial coordination environment found in thiol dioxygenases.[15,22–25] We elected to use the ligand 1,4,7-triazacyclononane (tacn) because it is a classical tridentate ligand platform used to study modern CDO model chemistry. For example, *N*-methyl and -isopropyl tacn derivatives were used to synthesize and characterize thiol dioxygenase model complexes capable of catalyzing S-oxygenation and disulfide formation.[22]

Here we report spectroscopic, electrochemical, and kinetic trends in a series of Fe(III)–thiolate intermediates capable of establishing S-N, S-O, and S-N-O binding modes. Intermediates are generated *in situ* within 37 °C buffered solution by combining aqueous [Fe(tacn)$Cl_3$] (**1(aq)**) with cysteamine or cysteamine analogues including penicillamine, mercaptopropionate, cysteine, *N*-acetylcysteine, and *N*-acetylcysteine methyl ester (Figure 2). We also report the synthesis and characterization of the most stable intermediate containing Fe(III)-bound penicillamine to better understand its coordination environment and electronic structure using FT-IR, NMR, and magnetic susceptibility measurements.

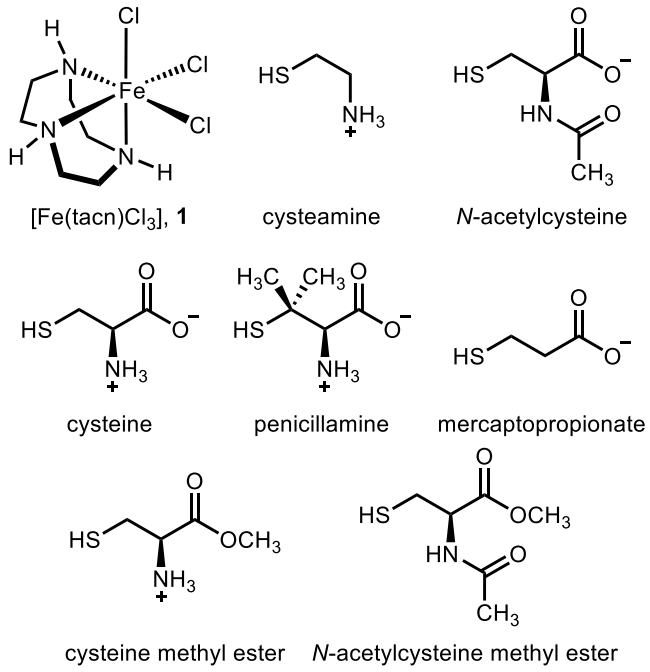


**Figure 2.** Structures of **1** and cysteamine analogues.

## EXPERIMENTAL SECTION

**General Methods.** All reagents were ACS reagent grade or better and used as received unless otherwise noted. Deionized water was purified to a resistivity of 18 Mohm•cm and used to prepare all solutions.

**Synthesis of [Fe(tacn)Cl$_3$] (1).** Following a reported procedure,[26] separate ethanolic solutions of 1,4,7-triazacyclononane (0.485 g, 3.75 mmol) and $FeCl_3 \cdot (H_2O)_6$ (1.160 g, 4.29 mmol) were combined to yield a yellow precipitate. The precipitate was isolated by vacuum filtration with a cold ethanol rinse and air dried to yield 1.029 g (94% yield) of **1** as a fine, yellow powder. Aqueous solutions of **1** are denoted as **1(aq)**.

**Synthesis of [Fe(tacn)(pen)]BPh$_4$ (2)**. L-Penicillamine (pen, 0.700 g, 4.69 mmol) and NaOH (0.295 g, 7.38 mmol) were combined and stirred in water (35 mL). After all solids dissolved, **1(aq)**

(0.100 L, 9.19 mM, 0.919 mmol) was added giving rise to a deep purple solution. After stirring for 5 min, aqueous $NaBPh_4$ (0.150 L, 58.4 mM, 8.77 mmol) was added to the purple solution producing a fine, blue precipitate. The reaction mixture was stirred in an ice bath for one hour before precipitate was isolated by centrifugation (50 mL conical tubes). Vacuum filtration is time consuming and not advised because the reaction mixture is relatively viscous (likely caused by excess $NaBPh_4$ in solution). Precipitate was rinsed with cold-water within centrifuge tubes and isolated by centrifugation to yield a blue powder. After drying under reduced pressure overnight, the blue powder was dissolved in a minimal volume of THF and precipitated by the addition of diethyl ether. Isolation by vacuum filtration yielded a dark purple powder. Yield = 0.329 g (55%). Selected IR bands (KBr pellet): $\nu$ ($cm^{-1}$) = 3242 (w, $\nu$(N-H)), 1646 (s, $\nu$(C=O)). $^1H$ NMR (400 MHz, $CD_3CN$, 17 °C): δ (ppm) 29.1, 19.2, 10.6, [7.28 (2H), 7.00 (2H), 6.85 (1H); tetraphenylborate counterion], 2.26 ($H_2O$), 1.94 (solvent residual peak), –3.0, –13.4, –20.9. Magnetic susceptibility balance: $\mu_{eff}$ = 1.67 $\mu_B$; Evans method (400 MHz, $CD_3CN$): $\mu_{eff}$ = 1.68 $\mu_B$. Anal. Calcd for $FeC_{35}H_{44}N_4O_2SB \cdot H_2O$: C, 62.79; H, 6.93; N, 8.37. Found: C, 62.17; H, 7.15; N, 7.99.

**Kinetics Measurements.** All kinetics measurements were performed under a $N_2$ atmosphere (2–4% $H_2$, < 1 ppm $O_2$) within an anaerobic chamber (Coy Laboratories). Solutions were prepared in degassed water. Reactions were performed in water, phosphate-buffered saline (10.0 mM phosphates, 137 mM NaCl, 2.7 mM KCl, pH 7.4), or *N*,*N*-bis(2-hydroxyethyl)-2-aminoethanesulfonate (BES) buffer (20 mM, pH 7.1 or 7.5). Kinetics experiments were initiated by heating separate solutions of substrate (10.0 mM) and **1(aq)** (1.00 mM) at 37 °C. While solutions were heating, a quartz cuvette (Starna Cells, Spectrosil Far UV Quartz Cuvette, 9B-Q-10) was heated at 37 °C within a UV-vis spectrophotometer (DeNOVIX DS-C). After heating for

20 min, 500 μL of each solution was added to the pre-heated quartz cuvette to initiate a reaction. UV-vis spectra were collected every 5 seconds over a 5-minute period, every 30 seconds over a 15-minute period, and every 2 minutes over a 40-minute period. Second-order rate constants were calculated using absorbance at 618 nm or 568 nm for reactions with cysteamine or all other substrates, respectively. Rate constant calculations were not performed for reactions with cysteine methyl ester or *N*-acetylcysteine methyl ester.

**Electrochemistry.** Cyclic voltammetry experiments were performed using Go Direct screen-printed electrodes (Vernier) featuring a carbon working electrode, carbon counter electrode, and Ag/AgCl reference electrode all of which are screen printed on a single substrate. The screen-printed electrode was used with a Go Direct (Vernier) potentiostat operated via Bluetooth within the same anaerobic chamber used for kinetics experiments ($N_2$ atmosphere, 2–4% $H_2$, < 1 ppm $O_2$). Acquisition parameters were two segments, an initial potential of –1,000 mV, switching potential of 500 mV, final potential of –1,000 mV, and a sweep rate of 750 mV/s. Samples were prepared by adding **1** (29.1 mg, 0.100 mmol) to a 10.0 mL solution of thiol substrate (10 mM) in buffer (20 mM BES, 138 mM NaCl, pH 7.5). The resulting solutions were mixed by swirling and the screen-printed electrode, which was rinsed in deionized water between measurements, was immediately placed into solution to record cyclic voltammograms.

**LC-MS.** Reactions were prepared in the same manner used for kinetics measurements except **1(aq)** and substrate had final concentrations of 10 and 20 mM, respectively. After 1 hour and still under an anaerobic atmosphere, solutions were transferred to a vial using a syringe and syringe-driven filter unit (0.2 micron, hydrophilic). Reaction solutions were analyzed by LC-MS (Agilent Technologies 1260 Infinity HPLC, Poroshell 120 EC-C18 2.7-micron column, and Agilent Technologies 6130 Quadrupole mass spectrometer).

**Physical Methods**. Elemental analyses were performed at Intertek Pharmaceutical Services in Whitehouse, NJ. Infrared (IR) spectra were obtained with a Perkin-Elmer Spectrum Two FT-IR spectrometer. $^{1}$H NMR spectra were collected in deuterated solvents using a Bruker Biospin Ascend 400 MHz spectrometer and referenced to residual solvent signal.

**Magnetic Susceptibility.** The effective magnetic moment of **2** was determined using a magnetic susceptibility balance (Johnson Matthey Mark I) and by the Evans NMR method.[27,28] Samples were prepared for the Evans method using a 5 mm coaxial insert (Norell) filled with a diamagnetic reference solution of $CD_3CN$ containing TMS (1.5% v/v). The outer NMR tube contained a solution of **2** (25.0 mM) in $CD_3CN$ containing TMS (1.5% v/v). The paramagnetic frequency shift of the TMS proton resonance in Hz was used to calculate the effective magnetic moment.

## RESULTS AND DISCUSSION

**Complex 1 forms reactive intermediates.** We selected tacn-chelated Fe(III) to mimic the facial N-donor atoms in thiol dioxygenase active sites, restrict exchangeable coordination sites on the metal center relative to non-chelated Fe(III), and to enable our reactions to occur in aqueous solution near physiological pH. We first tested if Fe(III)–thiolate intermediates form when starting from **1** in deionized water (effectively generating **1(aq)**). Mixing aqueous solutions of **1(aq)** and excess substrate (1:10 Fe/substrate) produced violet ($\lambda_{max}$ = 568 nm) intermediates with cysteine, penicillamine, *N*-acetylcysteine, and mercaptopropionate while blue ($\lambda_{max}$ = 618 nm) intermediates were produced using cysteine methyl ester and cysteamine. No colorimetric changes were observed using the negative control *N*-acetylcysteine methyl ester. Purple and blue intermediates decayed to colorless solutions, but color was reestablished upon aeration. The ability to regenerate intermediates upon aeration suggests intermediates decay to generate Fe(II) consistent with an

autoredox reaction. Catalytic turnover of intermediates under aerobic conditions interferes with kinetic measurements. Accordingly, we elected to perform all subsequent reactions and kinetics experiments under an anaerobic atmosphere to avoid aerobic oxidation of Fe(II) to Fe(III). After confirming **1(aq)** generates transient intermediates similar to previous reports using non-chelated Fe(III), we turned to selecting a suitable buffer for kinetics measurements.

Previous reports of Fe(III)–thiolate reaction kinetics used acidic or alkaline conditions to solubilize non-chelated Fe(III) ions.[17–20] Kinetics experiments using Fe(III) in aqueous media cannot be easily performed near physiological pH because hydrolysis of aquated Fe(III) precipitates the metal ion as hydroxide salts. It is well known that Fe(III) near pH ~7 requires supporting ligands to maintain solubility. Indeed, dissolving **1** in aqueous solution (in low mM range) near neutral pH produces a clear, yellow solution. It should be noted that **1(aq)** appears to induce water hydrolysis over the course of approximately 6 hours. Over this period **1(aq)** transitions to a clear, orange solution. It therefore appears the facial coordination mode of tacn slows the rate of water hydrolysis relative to non-chelated Fe(III) while also preventing olation and precipitation near neutral pH. To avoid the formation of hydrolysis products, we prepared fresh solutions of **1(aq)** at most 2 hours from the start of each kinetics experiment. These qualitative observations suggested the use of tacn-chelated Fe(III) permits the study of Fe(III)–thiolate reactivity near neutral pH.

**Optimizing a buffer system for kinetics experiments.** Motivated by the hydrolytic stability of **1(aq)** near neutral pH, we optimized buffer conditions for kinetics experiments. Early attempts with Tris-HCl (pH 8.0) and phosphate-buffered saline (pH 7.4) revealed limitations with these buffer systems. Near pH 8 cysteine methyl ester converts to cysteine by ester hydrolysis which appears as a gradual blue-shifting of the absorbance maximum during intermediate decay

(Figure S1). Given the propensity of cysteine methyl ester to undergo hydrolysis, we elected to pursue S-N binding mode experiments using cysteamine. However, phosphate buffer prevents the formation of both cysteine methyl ester and cysteamine intermediates. To avoid phosphate interference, we turned to a sulfonate-based buffer, *N*,*N*-bis(2-hydroxyethyl)-2-aminoethanesulfonate (BES), due to its suitable buffer range ($pK_a$ = 7.1) and relatively weakly coordinating sulfonate group. We did not observe intermediate formation using cysteamine and **1** in BES buffer at pH 7.1, but a blue intermediate formed at pH 7.5. Interestingly, CDO exhibits optimal cysteine binding at pH ~7.4.[3] Collectively, these results indicated BES buffer at pH 7.5 is a suitable system for measuring autoredox reaction rates.

**Substrate binding mode controls autoredox kinetics.** To measure the influence of S, N, and O binding modes on Fe(III)–thiolate autoredox rates, we mixed **1(aq)** with thiol substrate (1:10 Fe/substrate) in pH 7.5 BES buffer at 37 °C under an anaerobic atmosphere and measured UV-vis absorbance as a function of time. Autoredox rates were calculated by measuring the linear regression slope of reciprocal absorbance maxima as a function of time. Reactions performed under these conditions generated disulfide products (see Figures S2 and S3 for representative data) and highly linear second-order rate plots exemplified by **1(aq)** + cysteine and **1(aq)** + cysteamine (Figure 3).

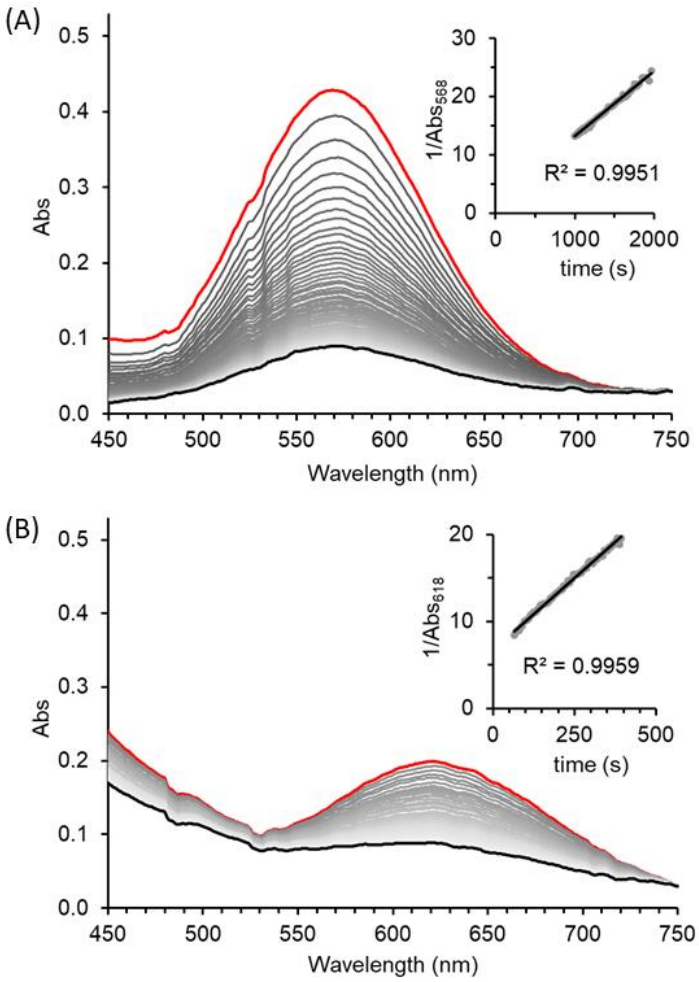


**Figure 3.** Representative UV–vis spectra of (A) **1(aq)** + cysteine and (B) **1(aq)** + cysteamine with (inset) corresponding reciprocal absorbance values plotted as a function of time. Reactions were performed anaerobically and contained **1(aq)** (0.500 mM) and substrate (5.00 mM) in BES buffer (pH 7.5) at 37 °C.

To evaluate trends in Fe(III)–thiolate autoredox rates, we compared second-order rate plots and their corresponding rate constants (Figure 4). Second-order rate plots illustrate Fe(III)–thiolate intermediates with relatively high, moderate, and low reactivity. The highly reactive intermediates formed from **1(aq)** combined with *N*-acetylcysteine, mercaptopropionate, or cysteamine. A common feature of these substrates is their capacity to form only monodentate or bidentate

interactions with Fe. No intermediate is observed between **1(aq)** and *N*-acetylcysteine methyl ester, a substrate limited to monodentate thiolate binding, suggesting that bidentate interactions occur in the series of highly reactive intermediates. Within the highly reactive series, *N*-acetylcysteine and mercaptopropionate produced the most reactive intermediates with autoredox rate constants of $18 \pm 1 \times 10^{-2}$ $M^{-1}$ $s^{-1}$ and $9.7 \pm 0.6 \times 10^{-2}$ $M^{-1}$ $s^{-1}$, respectively, while the cysteamine intermediate decayed with a rate constant of $4.8 \pm 0.7 \times 10^{-2}$ $M^{-1}$ $s^{-1}$. Interestingly, both *N*-acetylcysteine and mercaptopropionate can form the S-O binding mode while cysteamine can form the S-N binding mode. Therefore, within the substrates investigated here, Fe(III)–thiolate autoredox is fastest in the S-O binding mode. Intermediates with moderate and low reactivity were formed from cysteine and penicillamine which decayed with rate constants of $1.137 \pm 0.003 \times 10^{-2}$ $M^{-1}$ $s^{-1}$ and $0.009 \pm 0.001 \times 10^{-2}$ $M^{-1}$ $s^{-1}$, respectively. A common feature among cysteine and penicillamine is the presence of thiol, amine, and carboxylate groups which makes S-N, S-O, or S-N-O binding modes possible. Given the likely bidentate binding of the highly reactive series, we interpret the relative stability of cysteine and penicillamine intermediates as evidence of tridentate binding. Given our observed trend in autoredox kinetics, we next turned to cyclic voltammetry to characterize the electrochemical properties of the Fe(III)–thiolate intermediates.

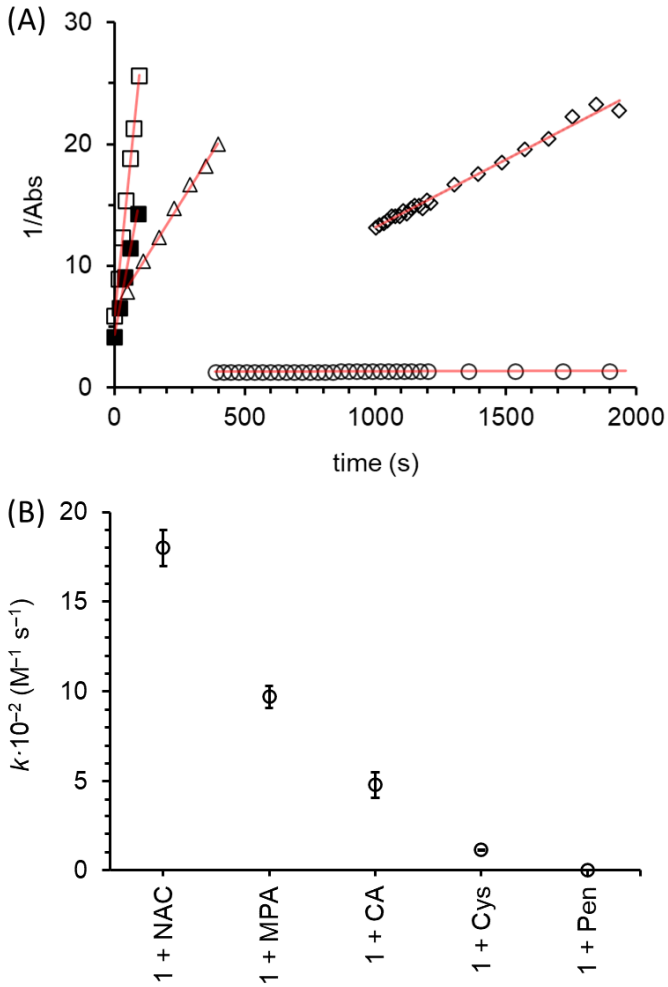


**Figure 4.** (A) Reciprocal absorbance as a function of time for **1(aq)** with *N*-acetylcysteine (□), mercaptopropionate (■), cysteamine (Δ), cysteine (◊), and penicillamine (○). Red lines represent linear regression fitting. (B) Second-order autoredox rate constants as a function of reaction **1(aq)** with *N*-acetylcysteine (NAC), mercaptopropionate (MPA), cysteamine (CA), cysteine (Cys), and penicillamine (Pen). Error bars represent standard error of the mean (n = 3). Reactions were performed anaerobically and contained **1(aq)** (0.500 mM) and substrate (5.00 mM) in BES buffer (pH 7.5) at 37 °C.

**Reduction potentials correlate with autoredox rates.** To measure electrochemical properties of Fe(III)–thiolate intermediates, we turned to cyclic voltammetry. We hypothesized that the most reactive intermediates contain the most oxidizing Fe(III) centers and would therefore exhibit the most positive reduction potentials. Cyclic voltammograms of **1(aq)** alone or with cysteamine analogues generally exhibit irreversible voltammograms, but intermediates generated with cysteine and penicillamine exhibit quasireversible characteristics (Figure 5). Given the irreversible or quasireversible nature of the cyclic voltammograms, we elected to compare cathodic peak potentials.

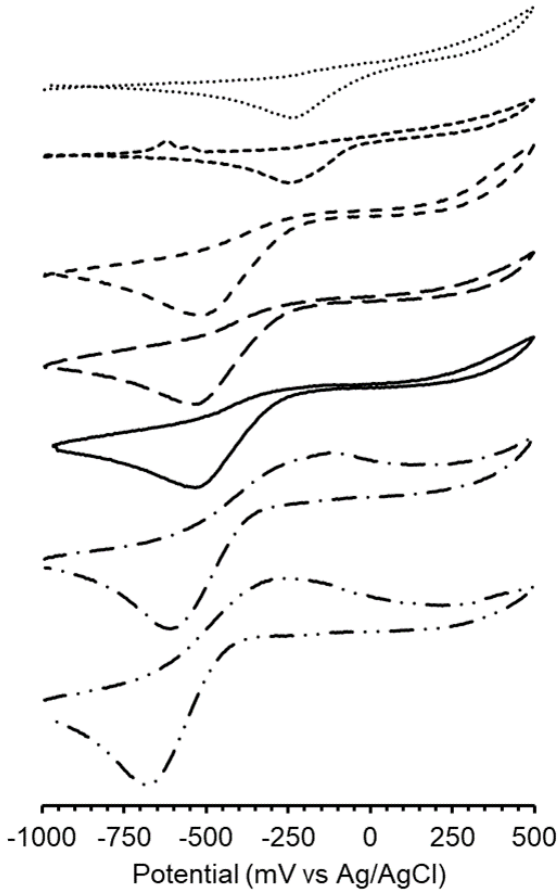

**Figure 5.** Cyclic voltammograms of solutions containing **1(aq)** (—) and **1(aq)** with *N*-acetylcysteine (···), mercaptopropionate (---), cysteamine (– – –), *N*-acetylcysteine methyl ester (— — —), cysteine (— · —), and penicillamine (— · · —). All samples are in BES buffer (20 mM BES, 138 mM NaCl, pH 7.5), were prepared and measured under anaerobic conditions ($N_2$ atmosphere, 2–4% $H_2$, < 1 ppm $O_2$), and were acquired with a 750 mV/s scan rate.

Comparing cathodic peak potentials with autoredox rate constants reveals a clear trend where more positive cathodic peak potentials correspond to more reactive Fe(III)–thiolate intermediates (Table 1). The most reactive intermediates generated with *N*-acetylcysteine and mercaptopropionate exhibit similar cathodic peak potentials but have significantly different autoredox rate constants. Similarly, the most stable intermediates generated with cysteine and penicillamine also exhibit similar cathodic peak potentials but significantly different autoredox rate constants. Interestingly, addition of an *N*-acetyl group to the beta-carbon of mercaptopropionate appears to accelerate autoredox while addition of methyl groups to the alpha-carbon of cysteine slows autoredox. These observations suggest that Fe(III)–thiolate autoredox rate constant is governed by electronic structure of the complex and by steric effects of the thiol substrate itself.

With respect to substrate binding mode, *N*-acetylcysteine methyl ester does not affect the cathodic peak potential of **1(aq)** suggesting no detectable binding interaction. This observation is in agreement with spectroscopic observations where *N*-acetylcysteine methyl ester did not produce a detectable S→Fe(III) charge transfer absorption when mixed with **1(aq)**. This negative control experiment suggests that a monodentate interaction alone is insufficient to generate a Fe(III)–thiolate intermediate. However, substrates capable of bidentate and tridentate binding modes clearly shift cathodic peak potentials to more positive and more negative values, respectively.

Accordingly, these electrochemical data support bidentate and tridentate binding modes in the Fe(III)–thiolate intermediates studied here. We next turned to attempting to isolate the most stable intermediates to better understand their coordination environment and electronic structure.

**Table 1.** Autoredox rate constants, cathodic peak potentials, and plausible binding modes for Fe(III)–thiolate intermediates and corresponding controls.

| Sample | Autoredox rate constant ($\times 10^{-2}$ $M^{-1}$ $s^{-1}$) | Cathodic peak potential (mV vs Ag/AgCl) | Plausible binding mode |
|---|---|---|---|
| **1(aq)** + *N*-acetylcysteine | 18 | –229 | S-O |
| **1(aq)** + mercaptopropionate | 9.7 | –242 | S-O |
| **1(aq)** + cysteamine | 4.8 | –521 | S-N |
| **1(aq)** + *N*-acetylcysteine methyl ester | N/A | –533 | N/A |
| **1(aq)** | N/A | –534 | N/A |
| **1(aq)** + cysteine | 1.1 | –611 | S-N-O |
| **1(aq)** + penicillamine | 0.009 | –675 | S-N-O |

**Isolation of a stable penicillamine intermediate.** To further investigate the binding mode of the intermediate formed by **1(aq)** and cysteine, we attempted to isolate it from aqueous solution. The cysteine intermediate appeared to precipitate from addition of aqueous sodium tetraphenylborate. However, the light blue precipitate immediately decomposed to yellow-green products in polar organic solvents, such as tetrahydrofuran and acetonitrile, making purification and characterization challenging. Given the structural similarity of cysteine and penicillamine and the apparent stability of the penicillamine intermediate, we reasoned that isolation and characterization of the penicillamine intermediate would be feasible and informative. Isolation of the penicillamine was achieved through precipitation with sodium tetraphenylborate to yield a light blue powder. The light blue powder was insoluble in water but soluble and moderately stable in tetrahydrofuran and acetonitrile yielding deep purple solutions. This observation suggested crude

**2** was isolated. Recrystallization of **2** from tetrahydrofuran with diethyl ether yields a dark purple powder. Elemental analysis of **2** suggests it is precipitated as a monohydrate with a formula [Fe(tacn)(pen)]$BPh_4 \cdot H_2O$. Having isolated penicillamine intermediate **2**, we next turned to characterization of its coordination environment and electronic structure.

To characterize the coordination environment of **2**, we performed infrared spectroscopy. The FT-IR spectrum of **2** contains notable features at 3433, 3242, and 1646 $cm^{-1}$ corresponding to hydrate O–H, tacn N–H, and penicillamine C=O frequencies, respectively (Figure S4). These assignments agree well with those previously reported for the Fe(III)-penicillamine complex Tl[Fe$(pen)_2$] (Figure 6).[29] In Tl[Fe$(pen)_2$] the penicillamine N–H and C=O frequencies are assigned at 3270 and 1640 $cm^{-1}$, respectively. We assign the stretch at 3242 $cm^{-1}$ as tacn N–H but do observe a shoulder at ~3275 $cm^{-1}$ which might arise from the penicillamine N–H stretch. Collectively, the FT-IR frequencies described here support the assignment of **2** containing penicillamine in the S-N-O binding mode (Figure 6). Moreover, given the similar structures of penicillamine and cysteine, it is likely that the cysteine intermediate also binds in the S-N-O mode. Collectively, these data suggest S-N-O binding mode decreases Fe(III)–thiolate autoredox rate relative to S-O and S-N binding modes. After characterizing vibrational features, we next sought to compare the electronic structure of **2** with those of thiol dioxygenase active sites.

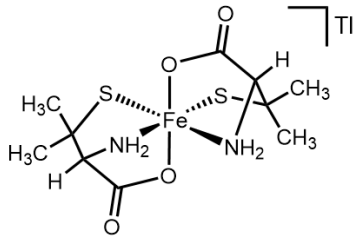


Tl[Fe$(pen)_2$]

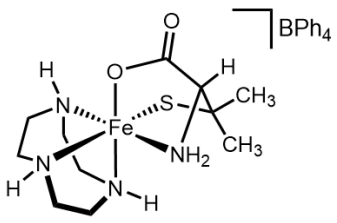


[Fe(tacn)(pen)]$BPh_4$, **2**

**Figure 6.** Structure of Tl[Fe(pen)$_2$], a crystallographically characterized complex containing penicillamine bound in the S-N-O mode,[29] and the proposed structure of complex **2**.

To characterize the electronic structure of **2**, we performed solid state and solution phase magnetic susceptibility measurements. Solid state measurements were performed using **2** in its powder form within a magnetic susceptibility balance and solution phase measurements were performed using the Evans NMR method. The effective magnetic moment calculated for solid and solution samples of **2** were 1.67 and 1.68 $\mu_B$, respectively, indicating that **2** contains a low spin ($S$ = ½) Fe(III) center. In agreement with this electronic structure determination is the NMR spectrum of **2** (Figure S5) featuring broad proton resonances spanning –30 to 30 ppm consistent with other low-spin Fe(III) complexes.[30] Collectively, these results indicate **2** contains penicillamine bound to low-spin Fe(III) and support the S-N-O binding mode interpretation for cysteine and penicillamine intermediates.

**Spectroscopic and electrochemical interpretation of substrate binding modes.** Intermediates generated from the reaction of **1(aq)** and cysteamine analogues unambiguously provide evidence of S-O, S-N, and S-N-O binding modes. Our interpretation is supported by the negative control reaction containing **1(aq)** and *N*-acetylcysteine methyl ester which does not generate a detectable S→Fe(III) charge transfer absorption and exhibits a cathodic peak potential nearly identical to **1(aq)** alone. The lack of spectroscopic and electrochemical change demonstrates that a thiol group alone is insufficient to generate a monodentate interaction under the conditions used in this study. In contrast, **1(aq)** and multidentate cysteamine analogues rapidly form S→Fe(III) charge transfer absorptions in solution and exhibit moderate-to-large shifts in cathodic peak potential relative to **1(aq)** alone. Intermediates formed with *N*-acetylcysteine and mercaptopropionate, both of which can bind Fe(III) in the S-O mode, are the fastest to decay by

autoredox and also exhibit the most positive cathodic peak potentials. The intermediate formed with cysteamine, which can bind Fe(III) in the S-N mode, exhibits a 50 nm blueshift in its S→Fe(III) absorption. A similar blueshift is observed with cysteine methyl ester, a substrate only capable of S-N binding, which therefore supports the S-N binding mode in the cysteamine intermediate. Intermediates formed with cysteine and penicillamine are most stable with respect to autoredox and have relatively negative cathodic peak potentials. Additionally, quasireversible cyclic voltammograms were only observed for these stable intermediates. These results strongly suggest cysteine and penicillamine preferentially bind in the S-N-O mode because binding in the S-O or S-N modes alone would likely produce positively shifted cathodic peak potentials and faster autoredox rates. Moreover, the isolated penicillamine intermediate exhibits similar vibrational stretching to a crystallographically characterized Fe(III) complex containing penicillamine bound in the S-N-O binding mode further supporting the tridentate binding mode interpretation. Collectively, our spectroscopic and electrochemical observations strongly support the assignment S-O, S-N, and S-N-O binding modes in the intermediates studied here.

**Results within the Context of ADO.** Our results must be carefully interpreted within the context of ADO autoredox chemistry because ADO likely binds cysteamine and mercaptopropionate in a monodentate fashion. However, there are several similarities between our results and characteristics of ADO. For example, the autoredox timescale of ADO-Fe(III) with cysteamine and the N-terminus of RGS5 is on the order of minutes, where ADO-Fe(III) is reduced to ADO-Fe(II) to some extent after 1 minute but nears completion after 10 minutes.[13] Our observations show a similar autoredox timescale for the intermediate generated from **1(aq)** + cysteamine where the S→Fe(III) charge transfer absorption decreases by ~50% after 1 minute and ~90% after 8 minutes. Therefore, the autoredox kinetics reported here might help rationalize

substrate-dependent autoredox rates of ADO. Given the similar autoredox timescales our system enables comparison of ADO-like autoredox chemistry in the absence of outer-sphere effects of the protein active site.

## CONCLUSION

We examined the effect of cysteamine analogue binding modes on Fe(III)–thiolate autoredox rates. Measuring autoredox reaction rates of a biomimetic complex is relevant to the chemistry of ADO because of its unique substrate selectivity and recently discovered autoredox chemistry. We elected to use model chemistry to measure autoredox rates and used **1** as a starting point because it contains a 3N facial coordination environment and exhibits moderate hydrolytic stability as **1(aq)** near neutral pH. Previous studies on Fe(III)–thiolate autoredox reactions used non-chelated Fe(III) necessitating acidic or alkaline solutions to maintain Fe(III) solubility. Thiol dioxygenases bind substrates in a physiologically relevant pH range, so results in acidic and alkaline solution are limited within the context of modeling ADO autoredox chemistry. We conclude that Fe(III)–thiolate autoredox rates and cathodic peak potentials depend on substrate binding mode where S-O > S-N > S-N-O. Furthermore, we observe autoredox reactivity on the same timescale reported for ADO autoredox activity. To support the assignment of cysteine and penicillamine binding in the S-N-O mode, we isolated the penicillamine-containing intermediate **2** as a tetraphenylborate salt. Complex **2** was characterized by elemental analysis, $^{1}$H-NMR, FT-IR, and magnetic susceptibility measurements suggesting penicillamine is bound to a low-spin Fe(III) center in the S-N-O mode.

Collectively, our experiments bridge the gap between seminal work on Fe(III)–thiolate autoredox kinetics and modern model chemistry using supporting ligands. These results will be

useful in rationalizing autoredox kinetics, reduction potentials, and spin states of ADO-Fe(III) and other non-heme Fe metalloenzymes exhibiting Fe(III)–thiolate autoredox chemistry.

AUTHOR INFORMATION

**Corresponding Author**

*Levi A. Ekanger, Department of Chemistry, The College of New Jersey, Ewing, NJ 08628, United States; orcid.org/0000-0001-8131-1641; Email: ekangerl@tcnj.edu; Webpage: www.ekangerchem.com

**Funding Sources**

The College of New Jersey

Dreyfus Foundation

ACKNOWLEDGMENT

This work was supported by The College of New Jersey (TCNJ) through faculty startup funds and through the Mentored Undergraduate Summer Experience (MUSE) program. The authors are also grateful for support from the Dreyfus Foundation through a Jean Dreyfus Lectureship for Undergraduate Institutions awarded to the TCNJ Department of Chemistry (Award BL-19-005). The authors acknowledge Mark O'Malley for assistance with creating a KBr pellet for FT-IR spectroscopy.

**REFERENCES**

[1] S. Aloi, C. G. Davies, P. A. Karplus, S. M. Wilbanks, G. N. L. Jameson, *Biochemistry* **2019**, *58*, 2398–2407.
[2] S. Aluri, S. P. de Visser, *J. Am. Chem. Soc.* **2007**, *129*, 14846–14847.
[3] J. A. Crawford, W. Li, B. S. Pierce, *Biochemistry* **2011**, *50*, 10241–10253.
[4] R. L. Fernandez, S. L. Dillon, M. H. Stipanuk, B. G. Fox, T. C. Brunold, *Biochemistry* **2020**, *59*, 2450–2458.

[5] R. L. Fernandez, N. D. Juntunen, B. G. Fox, T. C. Brunold, *J Biol Inorg Chem* **2021**, *26*, 947–955.
[6] C. R. Simmons, Q. Liu, Q. Huang, Q. Hao, T. P. Begley, P. A. Karplus, M. H. Stipanuk, *Journal of Biological Chemistry* **2006**, *281*, 18723–18733.
[7] Y. Wang, I. Shin, J. Li, A. Liu, *Journal of Biological Chemistry* **2021**, *297*, 101176.
[8] J. E. Dominy, C. R. Simmons, L. L. Hirschberger, J. Hwang, R. M. Coloso, M. H. Stipanuk, *Journal of Biological Chemistry* **2007**, *282*, 25189–25198.
[9] M. Fellner, E. Siakkou, A. S. Faponle, E. P. Tchesnokov, S. P. de Visser, S. M. Wilbanks, G. N. L. Jameson, *J Biol Inorg Chem* **2016**, *21*, 501–510.
[10] J. G. McCoy, L. J. Bailey, E. Bitto, C. A. Bingman, D. J. Aceti, B. G. Fox, G. N. Phillips, *Proc. Natl. Acad. Sci. U.S.A.* **2006**, *103*, 3084–3089.
[11] N. J. York, M. M. Lockart, S. Sardar, N. Khadka, W. Shi, R. E. Stenkamp, J. Zhang, P. D. Kiser, B. S. Pierce, *Journal of Biological Chemistry* **2021**, *296*, 100492.
[12] B. S. Pierce, B. P. Subedi, S. Sardar, J. K. Crowell, *Biochemistry* **2015**, *54*, 7477–7490.
[13] Y. Wang, I. Davis, Y. Chan, S. G. Naik, W. P. Griffith, A. Liu, *Journal of Biological Chemistry* **2020**, *295*, 11789–11802.
[14] N. Masson, T. P. Keeley, B. Giuntoli, M. D. White, M. L. Puerta, P. Perata, R. J. Hopkinson, E. Flashman, F. Licausi, P. J. Ratcliffe, *Science* **2019**, *365*, 65–69.
[15] M. Sallmann, B. Braun, C. Limberg, *Chem. Commun.* **2015**, *51*, 6785–6787.
[16] D. J. Fraser-Pitt, D. K. Mercer, D. Smith, A. Kowalczuk, J. Robertson, E. Lovie, P. Perenyi, M. Cole, M. Doumith, R. L. R. Hill, K. L. Hopkins, N. Woodford, D. A. O'Neil, *Infect Immun* **2018**, 86:e00947–17.
[17] R. F. Jameson, W. Linert, A. Tschinkowitz, V. Gutmann, *J. Chem. Soc., Dalton Trans.* **1988**, 943–946.
[18] R. F. Jameson, *J. Chem. Soc., Dalton Trans.* **1988**, 2109–2112.
[19] R. F. Jameson, W. Linert, *Monatsh. Chem.* **1991**, *122*, 887–906.
[20] M. J. Sisley, R. B. Jordan, *Inorg. Chem.* **1995**, *34*, 6015–6023.
[21] A. A. Fischer, J. R. Miller, R. J. Jodts, D. M. Ekanayake, S. V. Lindeman, T. C. Brunold, A. T. Fiedler, *Inorg. Chem.* **2019**, *58*, 16487–16499.
[22] J. B. Gordon, J. P. McGale, J. R. Prendergast, Z. Shirani-Sarmazeh, M. A. Siegler, G. N. L. Jameson, D. P. Goldberg, *J. Am. Chem. Soc.* **2018**, *140*, 14807–14822.
[23] J. B. Gordon, A. C. Vilbert, I. M. DiMucci, S. N. MacMillan, K. M. Lancaster, P. Moënne-Loccoz, D. P. Goldberg, *J. Am. Chem. Soc.* **2019**, *141*, 17533–17547.
[24] A. C. McQuilken, D. P. Goldberg, *Dalton Trans.* **2012**, *41*, 10883–10899.
[25] A. C. McQuilken, Y. Jiang, M. A. Siegler, D. P. Goldberg, *J. Am. Chem. Soc.* **2012**, *134*, 8758–8761.
[26] K. Wieghardt, K. Pohl, W. Gebert, *Angew. Chem. Int. Ed.* **1983**, *22*, 727–727.
[27] D. F. Evans, *J. Chem. Soc.* **1959**, 2003–2005.
[28] D. F. Evans, D. A. Jakubovic, *J. Chem. Soc., Dalton Trans.* **1988**, 2927–2933.
[29] A. Muller, M. Straube, E. Krickemeyer, H. Bogge, *Naturwissenschaften* **1992**, *79*, 323–325.
[30] P. B. Tsitovich, F. Gendron, A. Y. Nazarenko, B. N. Livesay, A. P. Lopez, M. P. Shores, J. Autschbach, J. R. Morrow, *Inorg. Chem.* **2018**, *57*, 8364–8374.